

## Full length article

## Regulation of cell attachment, spreading, and migration by hydrogel substrates with independently tunable mesh size

Jing Xia<sup>a,1</sup>, Zong-Yuan Liu<sup>b,1</sup>, Zheng-Yuan Han<sup>a</sup>, Yuan Yuan<sup>a</sup>, Yue Shao<sup>b</sup>, Xi-Qiao Feng<sup>b,\*</sup>, David A. Weitz<sup>a,c,\*\*</sup><sup>a</sup> School of Engineering and Applied Sciences, Harvard University, Cambridge, MA 02138, USA<sup>b</sup> Department of Engineering Mechanics, Institute of Biomechanics and Medical Engineering, Tsinghua University, Beijing 100084, China<sup>c</sup> Department of Physics, Harvard University, Cambridge, MA 02138, USA

## ARTICLE INFO

## Article history:

Received 9 October 2021

Revised 25 December 2021

Accepted 13 January 2022

Available online 15 January 2022

## Keywords:

Cell behavior

Hydrogel substrates

Mesh size

Stiffness

hBMSC

YAP

## ABSTRACT

Hydrogels are widely used as substrates to investigate interactions between cells and their microenvironment as they mimic many attributes of the extracellular matrix. The stiffness of hydrogels is an important property that is known to regulate cell behavior. However, since the mesh size of hydrogel is intrinsically coupled to its stiffness, its role in regulating cell behavior has never been independently investigated. Here, we report a hydrogel system whose mesh size and stiffness can be independently controlled. Cell behavior, including spreading, migration, and formation of focal adhesions is significantly altered on hydrogels with different mesh sizes but with the same stiffness. At the transcriptional level, hydrogel mesh size affects cellular mechanotransduction by regulating nuclear translocation of yes-associated protein. These findings demonstrate that the mesh size of a hydrogel plays an important role in cell-substrate interactions.

## Statement of significance

Hydrogels are ideal platforms with which to investigate interactions between cells and their microenvironment as they mimic many physical properties of the extracellular matrix. However, the mesh size of hydrogels is intrinsically coupled to their stiffness, making it challenging to investigate the contribution of mesh size to cell behavior. In this work, we use hydrogel-on-glass substrates with defined thicknesses whose stiffness and mesh size can be independently tuned. We use these substrates to isolate the effects of mesh size on cell behavior, including attachment, spreading, migration, focal adhesion formation and YAP localization in the nucleus. Our results show that mesh size has significant, yet often overlooked, effects, on cell behavior, and contribute to a further understanding of cell-substrate interactions.

Published by Elsevier Ltd on behalf of Acta Materialia Inc.

## 1. Introduction

Cells interact and respond to their local extracellular microenvironment. It not only serves as an essential physical scaffold for the cells, but it also provides a variety of stimuli that regulate cell behavior [1]. Hydrogels can mimic the attributes of the extracellular microenvironment while allowing control of their mechanical

and structural properties [2]; thus they are often used as a material with which to investigate the effects of these properties on cell behavior [3–5]. One of the most important and widely studied physical properties is the stiffness of hydrogel substrate. It is a key mechanical cue that regulates cell behavior and determines stem cell fate [6–9]. However, substrate stiffness cannot be the only parameter controlling cell behavior. Evidence has emerged that structural cues are of essential importance in guiding cell response [10,11]. For example, the decrease of the hydrogel mesh size can induce significant osteogenic differentiation of human stem cells [12]. However, contradictory results have reported that osteogenic and adipogenic differentiation of human stem cell is not affected by varying the mesh size of hydrogel [13]. This debate arises from the fact that the mesh size of the hydrogel is intrinsically coupled with the stiffness [14–17], making it very difficult to investigate

\* Corresponding author at: Department of Engineering Mechanics, Tsinghua University, Beijing 100084, China.

\*\* Corresponding author at: School of Engineering and Applied Sciences, Harvard University, Cambridge, MA 02138, USA.

E-mail addresses: [fengxq@tsinghua.edu.cn](mailto:fengxq@tsinghua.edu.cn) (X.-Q. Feng), [weitz@seas.harvard.edu](mailto:weitz@seas.harvard.edu) (D.A. Weitz).

<sup>1</sup> These authors contributed equally to this work.

the independent contribution of hydrogel mesh size to cell behavior. Furthermore, most studies have focused only on longer-term response such as cell differentiation, which happens over weeks, while how the mesh size affects shorter-term responses, such as attachment, spreading, and migration, which happen over hours to a few days, have been overlooked. To distinguish the contribution of mesh size, it is of critical importance to decouple the effects of mesh size and stiffness; this will enable investigation of the corresponding cell behavior such as attachment, spreading, and migration.

In this study, we report a hydrogel system whose stiffness and mesh size can be independently controlled, thereby, enabling us to isolate the effect of mesh size on the behavior of human bone marrow-derived mesenchymal stem cells (hBMSCs). By attaching the hydrogel with a defined thickness to the surface of a solid glass slide, we fabricate a hydrogel-on-glass substrate. The stiffness of this composite substrate is determined by a combination of the thickness and mesh size of the hydrogel layer; thus, by varying the thickness and the monomer concentration, the stiffness and mesh size of the hydrogel-glass substrate can be adjusted independently. We then grow cells on these substrates with the same stiffness but different mesh sizes, and investigate their behavior, including attachment, spreading, and migration. We find that the attachment of cells is not sensitive to the changes in hydrogel mesh size. By contrast, as the mesh size of hydrogel decreases, cells have significantly larger spreading areas and nuclear projected areas. Furthermore, cells migrate much faster on hydrogels with smaller mesh sizes. At the subcellular scale, cells form bigger focal adhesions on the hydrogels with smaller mesh sizes, indicating better adhesion between cells and hydrogels. Furthermore, we show that more yes-associated protein (YAP) translocates from the cytoplasm to the nucleus in the cells grown on the hydrogels with smaller meshes, indicating a regulatory role of hydrogel mesh size in the cellular mechanotransduction. These results demonstrate that the mesh size of hydrogel has significant effects on cell behavior and plays an important role in the cell-substrate interaction.

## 2. Materials and methods

### 2.1. Fabrication of hydrogel-on-glass substrates with defined thicknesses

Glass slides are functionalized using (3-Aminopropyl)triethoxysilane (APTES; Sigma-Aldrich, MO, USA) to facilitate covalent attachment of the hydrogel to glass. Briefly, glass slides are cleaned for 60 s using plasma cleaner (Diener electronic GmbH + Co. KG, Germany) at the power of 100 mW. The glass slides are then immersed in ethanol (Sigma-Aldrich, MO, USA) containing 1% APTES and 1% 1 M NaOH (Sigma-Aldrich, MO, USA) for 10 min. The glass slides are subsequently washed with ethanol twice and rinsed with deionized water. The glass slides are left at room temperature until completely dried.

A prepolymer solution is prepared with a total volume of 1124  $\mu\text{L}$  containing acrylamide monomers (Sigma-Aldrich, MO, USA), N, N'-Methylene-bisacrylamide (Sigma-Aldrich, MO, USA), 15  $\mu\text{L}$  of 10% weight percentage ammonium persulfate (Sigma-Aldrich, MO, USA), 0.5  $\mu\text{L}$  N, N, N', N'-tetramethylethylenediamine (Sigma-Aldrich, MO, USA) and beads of different diameters in deionized water. To tune the mesh size of the hydrogel, acrylamide monomer and N,N'-Methylenebisacrylamide are prepared at final weight percentages of 6% / 0.35%, 9% / 0.126%, and 12% / 0.065% in the prepolymer solution. To adjust the thickness of the hydrogel (2.5  $\mu\text{m}$ , 15  $\mu\text{m}$ , 30  $\mu\text{m}$ , and 200  $\mu\text{m}$ ), beads of different diameters are added to the prepolymer solution, which are 2.5  $\mu\text{m}$  (Magsphere, CA, USA), 15  $\mu\text{m}$  (Bangslab, Indiana, USA), 30  $\mu\text{m}$  (Sigma-Aldrich, MO, USA), and 200  $\mu\text{m}$  (Sigma-Aldrich, MO,

USA). The density of the beads is controlled such that the distance between the beads is at least 300  $\mu\text{m}$ . To fabricate thick hydrogels (1000  $\mu\text{m}$ ), we add plastic spacers of 1000  $\mu\text{m}$  at the edge of the coverslip. The prepolymer solution is then transferred to the pre-treated glass slides and then covered with 18-mm diameter coverslips. Two magnets, one on the top of the coverslip, one beneath the bottom of the glass slide, are used to press the coverslip and slide. After 3 h, the coverslip is gently peeled off and hydrogels are immersed in phosphate-buffered saline solution (Sigma-Aldrich, MO, USA).

### 2.2. DNA gel electrophoresis

Ultra-Low Range DNA Ladder (Thermo Scientific, MA, USA) is mixed with TriTrack DNA Loading Dye (contains Xylene Cyanol FF, Bromophenol Blue, and Orange G) (Thermo Scientific, MA, USA) and run through polyacrylamide electrophoresis hydrogels in TAE buffer at 110 V for 30 min. The samples are stained with GelRed Nucleic Acid Stain (Sigma-Aldrich, MO, USA) and imaged with a homemade imaging system built with a camera, a PC, and a UV/white light dual-light source.

### 2.3. Measurement of the Young's modulus of hydrogels

Polyacrylamide hydrogels are polymerized into cylindrical-disk shapes with 35 mm diameter and 10 mm thickness using petri dishes as molds. The hydrogel samples are immersed in PBS for at least 3 h such that the swelling of the hydrogel can reach its equilibrium. Nanoindentation measurements are performed using a nanoindenter (Agilent G200, Agilent Technologies, Santa Clara, USA) with a 100- $\mu\text{m}$ -diameter cylindrical diamond probe. For each composition of hydrogels, two samples are prepared and six individual measurements are performed on each sample at different locations, with at least a 200- $\mu\text{m}$  distance between two neighboring locations. Young's modulus is obtained from the continuous stiffness measurement (CSM) mode of the instrument at an amplitude of 500 nm and a frequency of 10 Hz.

### 2.4. Atomic force microscopy

The stiffness of the hydrogel-on-glass substrate with defined thickness is measured with an atomic force microscope (Nanowizard; JPK, Berlin, Germany). Silicon nitride cantilevers with spherical tips of 3.5  $\mu\text{m}$  diameter (NanoAndMore USA Corporation, CA, USA) are used. The hydrogel samples are immersed in PBS for at least 3 h such that their swelling can reach equilibrium. Samples are indented at 9 positions with a distance of at least 17  $\mu\text{m}$  apart between two neighboring positions. Samples are indented at an approach velocity of 5  $\mu\text{m/s}$  until a 2 nN trigger force is registered, and the tip is then retracted at 5  $\mu\text{m/s}$ . The linear portion of the indentation force–depth curve is analyzed with the JPK data processing software to extract the stiffness of the sample by fitting the indentation curve with the Hertzian model.

### 2.5. Functionalization of the substrate with collagen

These substrates are coated with collagen such that the cells can attach to the substrate well. Briefly, the samples are immersed in Hepes buffer (pH 8.5, Sigma-Aldrich, MO, USA) and then sterilized under germicidal light in a cell culture hood for 20 min. Then the samples are immersed in 0.125 mg/ml N-sulphosuccinimidyl-6-(4'-azido-2'-nitrophenylamino) hexanoate (sulfo-SANPAH; Thermo Scientific, MA, USA), activated with 365 nm UV light (Analytik Jena, Germany), washed, and then incubated overnight in 200  $\mu\text{g/ml}$  rat type-I collagen solution (Sigma-Aldrich, MO, USA).

## 2.6. Immunofluorescence staining of collagen

Substrates with collagen coating are blocked with 1% bovine serum albumin (Sigma, MO, USA) in PBS for 1 h, followed by a two-step immunostaining process. Briefly, the samples are first incubated with mouse monoclonal anti-collagen I antibodies (ab90395, Abcam, MA, USA) diluted 200X in PBS with a supplement of 1% bovine serum albumin for 1 h at room temperature. Samples are then washed 5 times with PBS and incubated with goat anti-mouse Alexa fluor plus 488 secondary antibodies (Thermo Fisher Scientific Inc, MA, USA) diluted 200X in PBS with a supplement of 1% bovine serum albumin for 1 h in the dark. Samples are washed 3 times with PBS before imaging. Substrate without collagen coating is stained with the same protocol as a negative control. The stained samples are then fluorescently imaged with a confocal microscope equipped with a 25X/0.95-NA water immersion objective (TCS-SP5; Leica Microsystems Inc., IL, USA).

## 2.7. Collagen quantification with enzymatic assay

To compare the collagen amount on the surface of the hydrogel, the ELISA kit (Chondrex, Inc. WA, USA) is partially adapted and the relative amount of collagen is determined based on changes in the optical density. Briefly, the samples are blocked with 1% BSA in PBS. The samples are then incubated with Peroxidase-Conjugated Goat Anti-Rat antibody at room temperature for 1 h. The samples are subsequently washed 3 times and incubated with TMB solution for 15 min. The stop solution is added to each sample and the optical density of the reacted solution is read at 450 nm.

## 2.8. Scanning electron microscopy

For observation of the hydrogel microstructure with a Scanning Electron Microscope (SEM), fixed samples are dehydrated in ethanol graded series (50%, 60%, 70%, 80%, 90%, 100%, Sigma, MO, USA) for 30 min each and eventually immersed in 100% ethanol for 2 h. After dehydration, samples are transferred to a critical point dryer (Tousimis 931GL, MD, USA) and dried under the critical point of CO<sub>2</sub>. Samples are then coated with 5 nm Pt/PD and observed with an Ultra 55 SEM (Carl Zeiss Microscopy, LLC, NY, USA).

## 2.9. Cell culture

Human bone marrow-derived mesenchymal stem cells (hBMSCs; ATCC, VA, USA) are used in this study. MSC growth medium is prepared by mixing mesenchymal stem cell basal medium (ATCC, VA, USA) with mesenchymal stem cell growth kit (ATCC, VA, USA). Cells are cultured in the MSC growth medium and maintained in the 37°C, 5% CO<sub>2</sub> infused incubator. All experiments are carried out with early passage hBMSCs (passage 2–passage 6).

## 2.10. Cell attachment and migration assay

Cells are seeded onto substrates at a density of ~4000 cells/cm<sup>2</sup> and cultured in MSC growth medium. Nuclei of cells are stained with 0.5 μM SiR-DNA staining reagents (Cytoskeleton Inc., DENVER, CO, USA). To perform the live-cell imaging, substrates with cells are kept in an incubator (OKO lab, NA, Italy) supplemented with 5% CO<sub>2</sub> and maintained at 37°C. The cells are imaged for continuous 4 days with a confocal microscope equipped with a 10X/0.3-NA dry objective (TCS-SP5; Leica Microsystems Inc., IL, USA).

## 2.11. Cell morphology assay

To observe the cell morphology, cells are seeded on substrates at a density of ~4000 cells/cm<sup>2</sup>. We fluorescently stain the cell cy-

toplasm with 2 μg/ml CellTracker™ green (Thermo Fisher Scientific Inc, MA, USA) and stain the cell nucleus with 0.5 μM SiR-DNA (Cytoskeleton Inc., DENVER, CO, USA). The stained cells are fixed with 4% formaldehyde and imaged with a confocal microscope equipped with a 25X/0.95-NA water immersion objective (TCS-SP5; Leica Microsystems Inc., IL, USA).

## 2.12. Immunofluorescence assay of focal adhesion

Cells are seeded on substrates at a density of ~4000 cells/cm<sup>2</sup> and cultured in an incubator infused with 5% CO<sub>2</sub> and maintained at 37 °C. After 16 h, cells are fixed with 4% formaldehyde and 0.1% Triton X100 diluted in PBS, followed by PBS wash 3 times to remove excessive reagents. Fixed cells are then triple stained for actin, vinculin, and nucleus: fixed cells are blocked with 10% normal goat serum (Thermo Fisher Scientific Inc, MA, USA) in PBS for 1 h, followed by a two-step immunostaining process for vinculin. Briefly, cells are first incubated with mouse monoclonal anti-vinculin antibodies (Sigma-Aldrich, MO, USA) diluted 200X in PBS with a supplement of 10% normal goat serum for 1 h at room temperature. Samples are then washed 5 times with PBS and incubated with goat anti-mouse Alexa fluor plus 488 secondary antibodies (Thermo Fisher Scientific Inc, MA, USA) diluted 200X in PBS with a supplement of 10% normal goat serum for 1 h in the dark. Phalloidin-iFluor 555 (Abcam, MA, USA) and Draq 5 nucleus probe (Thermo Fisher Scientific Inc, MA, USA) are diluted at ratios of 1:1000 and 1:5000 each to stain actin and nuclei of cells. Stained cells are washed 3 times with PBS and imaged with a confocal microscope equipped with a 63X/1.20-NA water immersion objective (TCS-SP5; Leica Microsystems Inc., IL, USA).

## 2.13. Immunofluorescence assay of YAP

Cells are seeded on substrates at a density of ~4000 cells/cm<sup>2</sup> and cultured in an incubator infused with 5% CO<sub>2</sub> and maintained at 37 °C. After 16 h, cells are fixed with 4% formaldehyde and 0.1% Triton 100X diluted in PBS, followed by PBS wash 3 times to remove excessive reagents. Fixed cells are triple stained for actin, YAP, and nucleus: fixed cells are blocked with 10% normal goat serum (Thermo Fisher Scientific Inc, MA, USA) in PBS for 1 h, followed by a two-step immunostaining process for YAP. Briefly, cells are incubated with rabbit polyclonal anti-YAP antibodies (Cell Signaling Technology, Inc., MA, USA) diluted 200X in PBS with a supplement of 10% normal goat serum for 1 h at room temperature. Samples are then washed 5 times with PBS and incubated with goat anti-rabbit Alexa fluor plus 594 secondary antibodies (Thermo Fisher Scientific Inc, MA, USA) diluted 200X in PBS with a supplement of 10% normal goat serum for 1 h in the dark. Phalloidin-iFluor 555 (Abcam, MA, USA) and Draq 5 nucleus probe (Thermo Fisher Scientific Inc, MA, USA) are diluted at ratios of 1:1000 and 1:5000 each to stain actin and nuclei of cells. Stained cells are washed 3 times with PBS and imaged with a confocal microscope equipped with a 63X/1.2-NA oil immersion objective (LSM880; Nikon Instruments Inc. NY, USA).

## 2.14. Image analysis

To quantify the collagen coating on substrates, the fluorescence intensity of the confocal images is measured with ImageJ (<https://imagej.nih.gov/ij/>). For the cell attachment study, the number of the cell nucleus is counted with the particle analyzer plugin in ImageJ. For the cell morphology study, fluorescence images of cells are segmented by OTSU's method; cell spreading area and nuclear projected area are further measured with particle analyzer plugin in ImageJ. For the cell migration study, fluorescent images of the cell nucleus are contiguously recorded with a 5 min interval. The

migration trajectories of cells are extracted by tracking their nuclei with the particle tracker plugin in ImageJ. The extracted trajectories are then analyzed with MATLAB (Mathworks, MA, USA) to calculate cell migration speed and directional persistence. Analysis of focal adhesions is performed according to a previous method [18]. For the YAP nuclear translocation study, the total fluorescence intensity of YAP in the nuclear and cytoplasmic regime are quantified with ImageJ.

### 2.15. Statistical analysis

Statistical analysis is performed using Origin software (Origin-Lab Corporation, MA, USA). The one-way analysis of variance (ANOVA) is used to determine whether there are any statistically significant differences between multiple comparisons [19]. *P*-values larger than 0.05 are assumed to be non-significant in all analyses; *P*-values smaller than 0.05 are assumed to be significant and marked with \*; *P*-values smaller than 0.01 are marked with \*\*; *P*-values smaller than 0.001 are marked with \*\*\*; *P*-values smaller than 0.0001 are marked with \*\*\*\*.

## 3. Results and discussion

### 3.1. Preparation of hydrogel substrates with different mesh sizes but the same stiffness

To decouple the stiffness of the hydrogel from its mesh size, we fabricate a composite substrate where a hydrogel of controlled thickness is cast on the surface of a rigid, glass slide. The stiffness of this composite substrate is determined by both the intrinsic stiffness of the hydrogel, which depends on its mesh size, and the thickness of the hydrogel layer. Then, by adjusting both the intrinsic stiffness of the hydrogel and its thickness, we can independently control the mesh size and stiffness of the composite substrate. We fabricate these composite substrates by casting polyacrylamide (PAA) hydrogel layers onto glass slides treated with 3-Aminopropyltriethoxysilane (APTES). The treatment of APTES on the glass slides enables strong covalent binding of the polyacrylamide (PAA) hydrogel to the glass slides. To ensure cells adhere to the hydrogels, we covalently couple type-I collagen molecules to the hydrogel surface using the heterobifunctional linker sulfo-succinimidyl 6-(4'-azido-2'-nitrophenylamino) hexanoate (sulfo-SANPAH), as shown in Fig. 1(a).

To change the mesh size of the hydrogel, we tune the concentrations of acrylamide monomer and crosslinker *N,N'*-Methylene-bisacrylamide, which are used for PAA hydrogel polymerization. We make three samples: one has a weight/volume percentage concentration of 6% monomer and 0.35% crosslinker; the other two have monomer/crosslinker weight/volume percentage concentrations of 9%/0.126%, and 12%/0.065%, respectively. To compare the mesh size of hydrogels, we freeze dry samples and observe them with scanning electron microscopy (SEM). The mesh size of the dried hydrogel decreases as the acrylamide concentration increases, as shown in Fig. 1(b). However, the value measured with SEM is likely an overestimation of the mesh size of the hydrogel in its hydrated state due to structural collapse during the sample drying process [12,13]. To qualitatively compare the mesh size among hydrogel samples, we measure the dynamics of DNA fragments passing through the hydrogels in their hydrated state by gel electrophoresis. The mobility of the DNA fragment is an indicator of the relative mesh size among hydrogel samples; higher mobility of the DNA fragment indicates a larger mesh size [20–22]. We fabricate the hydrogels following the same protocol as those for SEM imaging but without drying them. We find that DNA fragments migrate faster in hydrogels with lower concentrations of acrylamide, as shown in Fig. 1(c). In addition, the same observation has been

made on the mobility of DNA loading dyes, as shown in Fig. S1. This suggests that hydrogels with lower concentrations of acrylamide have larger mesh sizes; the relative size of hydrogel mesh is also consistent with those measured with SEM. Taken together, all three measurements are consistent and confirm that the mesh size of the hydrogel decreases as the acrylamide concentration increases from 6% to 12%.

The variation of hydrogel mesh size with composition also leads to a variation in the intrinsic stiffness of the hydrogel. To determine the intrinsic stiffness of the hydrogel, we fabricate a thick layer (~10 mm) of the polyacrylamide hydrogel and measure its intrinsic stiffness with a nanoindenter. As the acrylamide concentration increases from 6% to 12%, the intrinsic stiffness, or Young's modulus of the hydrogel, decreases from ~15 kPa to ~7.5 kPa, as shown in Fig. S2. To adjust the stiffness of the composite substrates, we fabricate hydrogel layers with different thicknesses onto the glass slides [23–25]. We use two different methods to vary the thickness of PAA hydrogel layers, either by adding spacer beads with a certain diameter [24] or by adding plastic spacers, as shown in Fig. 1a. For the spacer beads, we intentionally control the density of the beads in the hydrogels such that the distance between the beads is at least 300  $\mu\text{m}$ , which is much larger than the size of a single cell (~80  $\mu\text{m}$ ). Therefore, when the cells are cultured on substrates, most of them do not contact beads and are not influenced by the beads. The stiffness of the hydrogel-glass substrate is measured with atomic force microscopy (AFM). A typical indentation force–depth curve of AFM measurement is shown in Fig. S3. For each of the different compositions, the stiffness decreases rapidly as the thickness increases, but saturates at the intrinsic stiffness of the hydrogel when the thickness is greater than 30  $\mu\text{m}$ , as shown in Fig. S4. To select the substrates with the same stiffness, we choose the overlapping stiffness range of hydrogel substrates with different mesh sizes, which is ~12–15 kPa. Therefore, we select three substrates with the same stiffness of ~13 kPa: 30  $\mu\text{m}$  thick PAA at an acrylamide concentration of 6%, 15  $\mu\text{m}$  thick PAA at 9%, and 2.5  $\mu\text{m}$  thick PAA at 12%. The stiffnesses of these three samples are very nearly the same, as shown in Fig. 1(d). Nevertheless, the mesh sizes are clearly distinct, as evidenced from Fig. 1(b) and (c). For simplicity, these three substrates are referred to as PAA 6%, PAA 9%, and PAA 12%, respectively. In this manner, hydrogel mesh size is the unique changing parameter and its effect on the cell behavior can be decoupled from the hydrogel stiffness.

### 3.2. Characterization of collagen coating on hydrogels with different mesh sizes

Cells do not readily attach to PAA hydrogels due to the lack of anchoring sites [26]; therefore, extracellular matrix (ECM) ligands, such as collagen, must be bound to the surface of the hydrogel to provide the essential anchoring sites for cells [27,28]. In this study, we coat the hydrogels with sulfo-SANPAH, a protein crosslinker, and then covalently link collagen molecules to the sulfo-SANPAH. The same concentration of sulfo-SANPAH and collagen are used for all the hydrogels.

To ensure that any observed differences in cell behavior do not originate from the ECM protein functionalization, the collagen coating of the hydrogels is interrogated using three methods: a direct fluorescence quantification assay, an immunostaining assay and an enzymatic assay. To perform the direct fluorescence quantification assay, we coat the hydrogel surface with a mixture of FITC-labeled and unlabeled collagen at a ratio of 5:1, and quantify the surface fluorescence with confocal microscopy according to a previously reported method [29–31]. We find that spot-like collagen is randomly distributed on all hydrogel surfaces, as shown in Fig. 2(a). This is in contrast to the rod-like fibers of collagen assem-



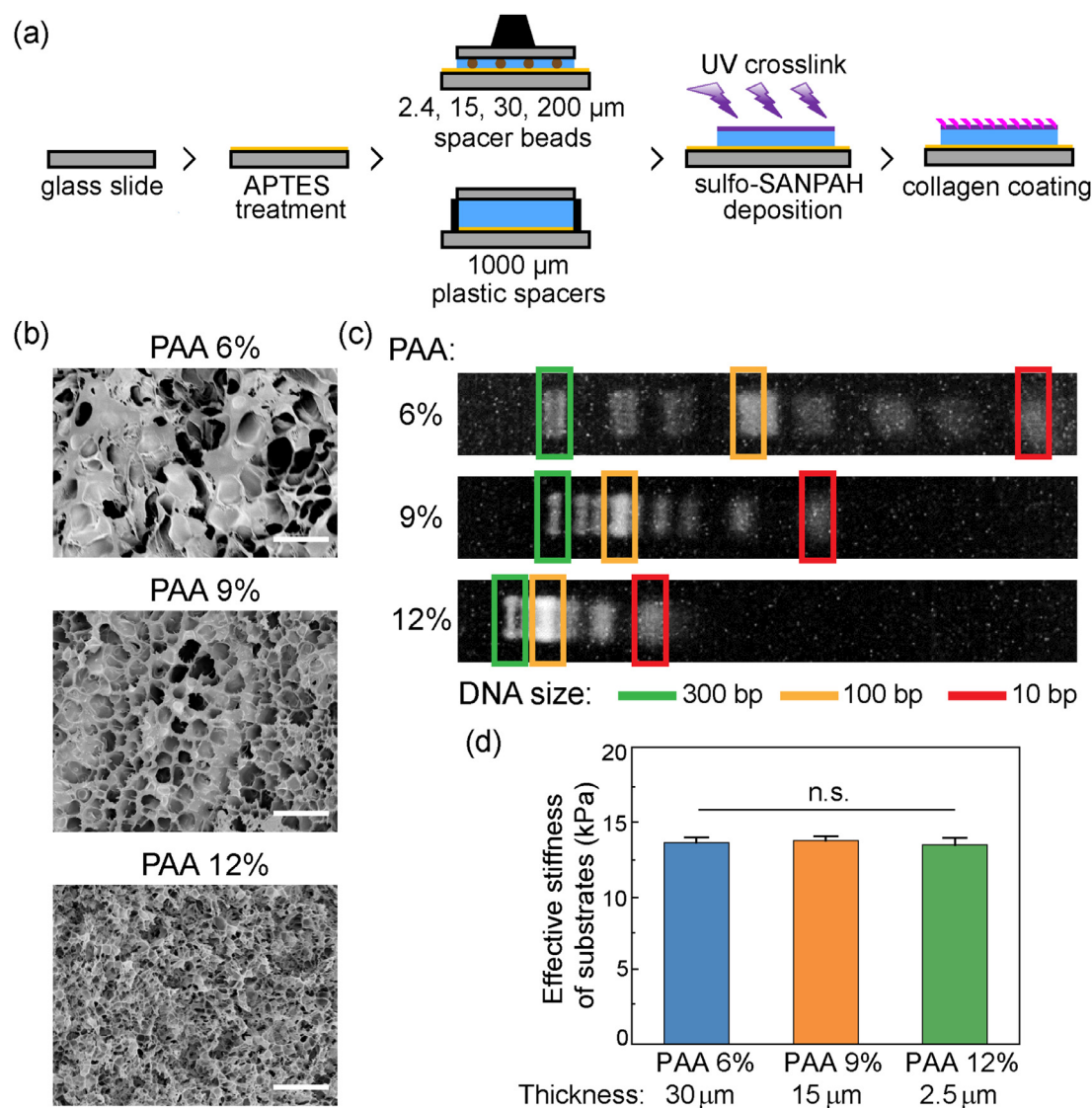


**Fig. 1.** Fabrication of hydrogel-on-glass substrates with different mesh sizes but the same stiffness. (a) Schematic of the fabrication workflow of hydrogel-on-glass substrates with defined thickness. (b) Representative SEM images of PAA hydrogels with different acrylamide concentrations. Scale bars, 5  $\mu\text{m}$ . (c) Electrophoresis of DNA fragments in hydrated PAA hydrogels with different acrylamide concentrations. (d) Stiffness of the hydrogel-on-glass substrates with indicated acrylamide concentrations and hydrogel thicknesses (Mean  $\pm$  SD,  $N = 9$  per group, one-way ANOVA,  $P > 0.05$ ).

bled under the physiological condition [32,33]. We attribute this difference to the deposition of sulfo-SANPAH on the PAA hydrogel surface, which disrupts fiber formation of collagen monomers due to the non-specific protein conjugation and the blockage of triple helices [34–36]. We then quantify the average fluorescence intensity of the collagen coatings among different samples. The fluorescence intensity of the collagen coating is nearly the same among samples with no obvious difference, as shown in Fig. 2(b). This conforms with the previous finding that the collagen coating does not change as the hydrogel structure changes [37,38]. To further confirm this result, we perform the second assay, an immunostaining assay. We coat the hydrogel surface with unlabeled collagen and immunofluorescence stain them, as shown in Fig. S5(a). We observe similar collagen structures and averaged fluorescence intensity among the collagen coating of hydrogels, as shown in Fig. S5(b). In the absence of any collagen coating, the measured fluorescence intensity is one order of magnitude smaller, confirming that the fluorescence measured is from the collagen coating, as shown in Fig. S6. To verify that the amount of the collagen coating quantified by the confocal imaging method is not biased by

the resolution of the imaging technique, we quantify the collagen coating of hydrogels with an enzymatic assay as the third method. Briefly, collagen coatings are incubated with peroxidase-conjugated collagen antibodies to allow them to bind; the amount of bound peroxidase-conjugated antibodies is proportional to the amount of collagen coating. We then add 3,3',5,5'-Tetramethylbenzidine (TMB) substrate to the samples and allow it to react with the peroxidase-conjugated collagen antibodies to produce a measurable color change, as depicted in Fig. 2(c). The optical density of the reaction product at 450 nm is used as an indicator of the collagen coating amount. The optical density values show no observable difference among different hydrogels, as shown in Fig. 2(d). Therefore, we conclude that no significant difference exists in collagen coatings across hydrogels with different mesh sizes.

### 3.3. Effects of hydrogel mesh size on the cell attachment

To investigate how cells respond to hydrogels with different mesh sizes, we culture cells on these different substrates and observe their corresponding behavior. The first behavior we investi-

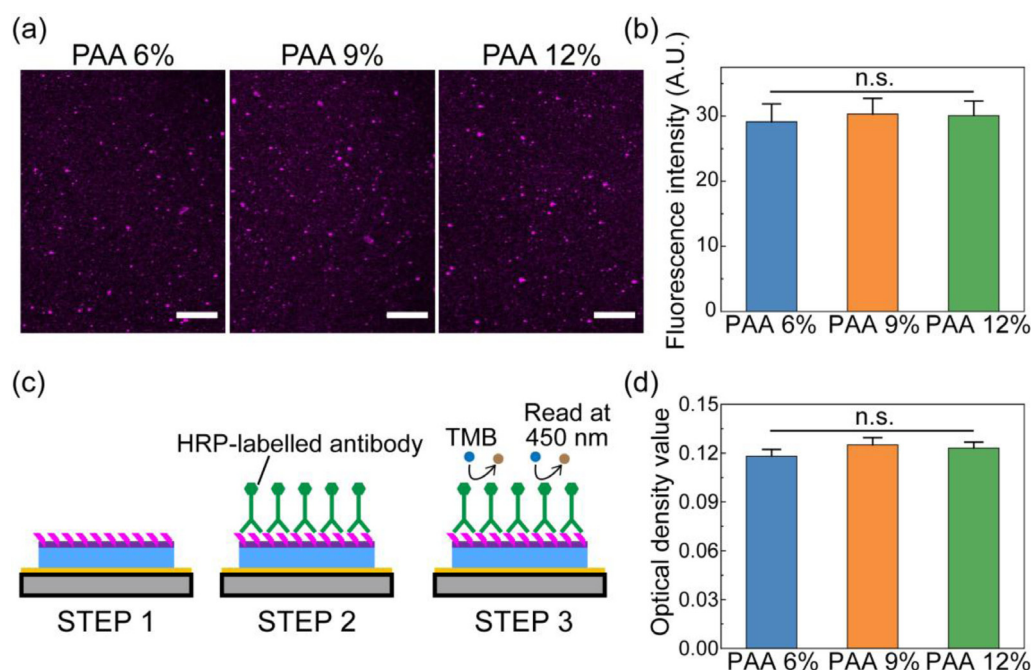


**Fig. 2.** Characterization of collagen coating on hydrogels. (a) Representative fluorescence images of FITC-labeled collagen on different hydrogels. Scale bars, 50  $\mu\text{m}$ . (b) The average fluorescence intensity of FITC-labeled collagen on different hydrogels (Mean  $\pm$  SD,  $N = 20$  per group, one-way ANOVA,  $p > 0.05$ ). (c) Schematic of the enzymatic detection assay of collagen coating on hydrogels. (d) Optical density values of peroxidase-TMB reaction product measured on different hydrogels (Mean  $\pm$  SD,  $N = 9$  per group, one-way ANOVA,  $p > 0.05$ ).

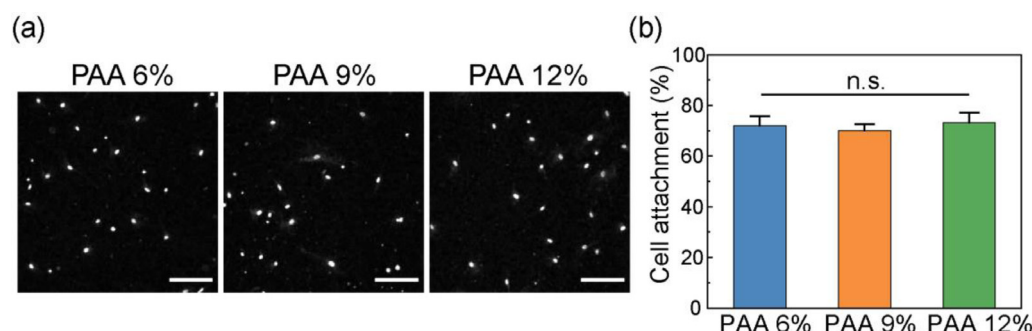


**Fig. 3.** Attachment of cells on hydrogels with different mesh sizes. (a) Representative confocal fluorescence microscopy images of cells on different hydrogels with nuclei stained; cells are imaged 12 h after they are seeded. Scale bars, 200  $\mu\text{m}$ . (b) Percentage cells attached on different hydrogels (Mean  $\pm$  SE,  $N = 26$  per group, one-way ANOVA,  $p > 0.05$ ).

gate is the cell attachment, which is the initial step in the cascade of cell-substrate interactions. Cells are seeded onto hydrogels at a low density of  $\sim 4000$  cells/ $\text{cm}^2$ , so that most cells are isolated, without cell-cell contact. Cells are well separated on different substrates, as shown by the representative confocal images in Fig. 3(a). The number of attached cells is quantified and normalized by the total cell number seeded in the medium to calculate the percentage of cells that are successfully attached to the substrates. For the conditions used in all experiments, at least 80% of the cells attach to the hydrogels, and no statistically significant difference in cell-attachment percentage is found among the different substrates, as shown in Fig. 3(b). We therefore conclude that the influence of the mesh size of the hydrogel on cell attachment is negligible. A possible interpretation of this observation is that the cell attachment is predominantly determined by the collagen coating on the hydrogel surface [39], for which we observe no differences under our experimental conditions.

### 3.4. Effect of hydrogel mesh size on the cell morphology

Shortly after their initial attachment, cells will stretch themselves and spread on the substrates. The morphology of the cell has important consequences on cell metabolism [40], as it can determine whether or not a cell proliferates [41], or dies [42]. We investigate the morphology of the fully spread cells on different substrates. We seed cells on the substrates at a low density of  $\sim 4000$  cells/ $\text{cm}^2$ . We fluorescently stain the cells with CellTracker<sup>TM</sup> green to determine their spreading area. We also fluorescently stain the nuclei with DNA dye DRAQ5 to determine their nuclear projected area; representative images obtained with confocal microscopy are shown in Fig. 4(a). Cell spreading area and nuclear projected area are quantified from the confocal microscopy images using ImageJ software. The results suggest that the cell spreading area is significantly larger on hydrogels with smaller mesh sizes, as shown in Fig. 4(b). However, the circularity of cells, defined as  $4\pi \times$

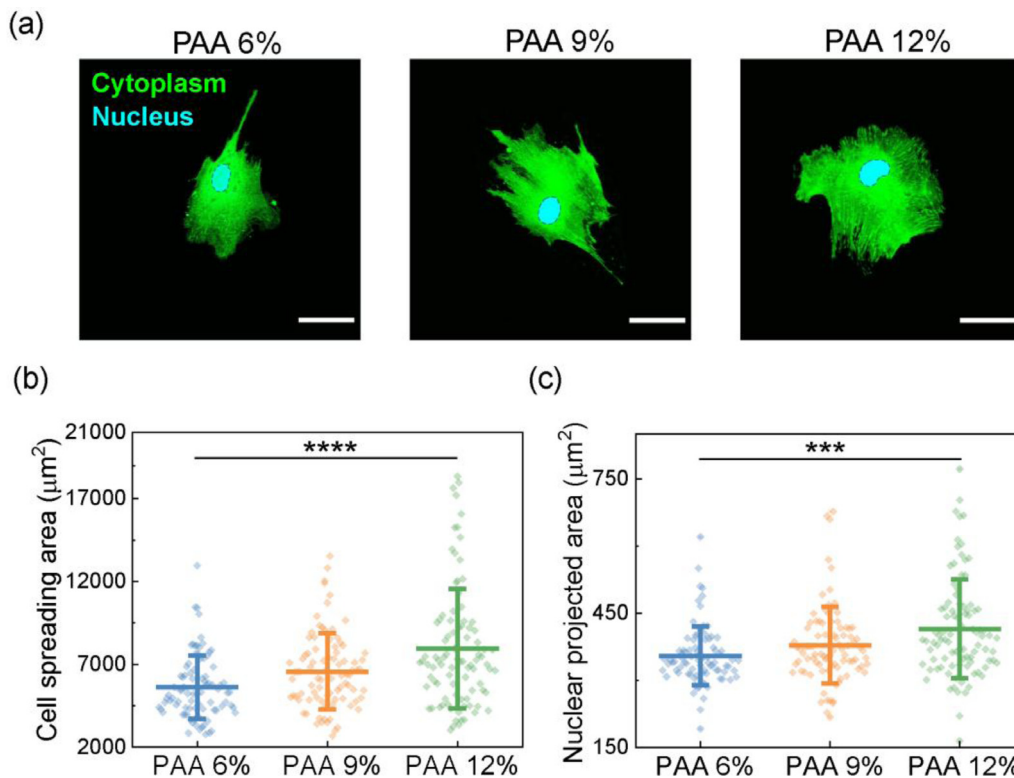


**Fig. 4.** Morphology of cells on hydrogels with different mesh sizes. (a) Representative confocal microscopy images of cells on different hydrogels. The cytoplasm of the cell is depicted in green; the nucleus of the cell is depicted in cyan. Scale bars, 50  $\mu\text{m}$ . (b) Cell spreading area on different hydrogels (Mean  $\pm$  SD,  $N > 88$  per group, one-way ANOVA,  $p < 0.0001$ ). (c) Nuclear projected area on different hydrogels (Mean  $\pm$  SD,  $N > 88$  per group, one-way ANOVA,  $p < 0.0001$ ).

Area/Perimeter<sup>2</sup>, exhibits no difference on hydrogels with different mesh sizes, as shown in Fig. S7. Moreover, the nuclear projected area follows the same trend as the cell spreading area, as shown in Fig. 4(c). Our results demonstrate that by varying the mesh size of the hydrogel, the spreading behavior of cells is pronouncedly altered. Interestingly, the same correlation between cell spreading and nuclear projected area is also reported for cells grown on substrates with different stiffnesses and microstructures [43–45], possibly indicating a similar regulating mechanism of hydrogel mesh size that determines the cell spreading and nuclear projected area.

### 3.5. Effect of hydrogel mesh size on the cell migration

Beside cell spreading, mechanical and structural cues also influence a series of other cell functions, in particular, cell migration, which is closely associated with cell attachment and spreading [46]. Cell migration is the dynamic movements of cells that is essential for morphogenesis and tissue remodeling [47,48]. To investigate cell migration on the hydrogels, cells are seeded sparsely enough to avoid cell-cell interactions and are imaged with confocal microscopy over 48 h. Trajectories of cell migration are extracted from the confocal images with Image-J software. Cells migrate in a random pattern without any directional preference and do so on hydrogels with different mesh sizes, as shown by the overlays of cell migration trajectories in Fig. 5(a). Our finding is in stark contrast with the directed motion of cells on fibrous collagen networks that results from the strong contact guidance of collagen fibers [49–51], suggesting that the random migratory behavior observed here likely results from the non-fiber structure of the collagen coating.

We then determine the efficiency of the cell migration, which depends on two essential parameters: migration speed and directional persistence, which quantifies the robustness of a cell moving

along the same direction. We first calculate the average migration speed of the cells, which is determined by dividing the contour length of the migration trajectory by its duration. We find that cells migrate faster on hydrogels with smaller meshes, as shown in Fig. 5(b). Additionally, we determine the distribution of the average migration speeds among cells; for all hydrogels, the distribution is broad and there is a slight shift in the shape, with more faster cells as the mesh size decreases, as shown in Fig. 5(c). The other determining parameter of the cell migration efficiency is the directional persistence, which is a parameter that quantifies the straightness of the trajectory and is determined by the ratio of the end-to-end distance to the contour length of each trajectory [52,53]. In contrast to the average migration speed, the directional persistence exhibits no difference among hydrogels with different mesh sizes, as shown in Fig. 5(d) and (e). These results suggest that cell migration efficiency is improved on hydrogels with smaller mesh sizes, which is caused by the increased migration speed, even though there is no change in directional persistence.

### 3.6. Effect of hydrogel mesh size on the formation of focal adhesions

Given the dramatic changes in the spreading and migration behavior of cells with different hydrogel mesh sizes, we hypothesize that there is a corresponding change in the focal adhesion, which is a key mechanosensor at the interface between the cell and the ECM and which plays a critical role in cell spreading and migration [54,55]. The focal adhesion serves as a bridge between the extracellular substrate and the cell, connecting the extracellular substrate at one end and actin stress fibers at the other, as shown schematically in Fig. 6(a). Both the focal adhesion and actin stress fibers are indicators of how strongly a cell binds to the substrate [56–58] and we therefore interrogate the morphology of these two cellular components. To characterize the mor-

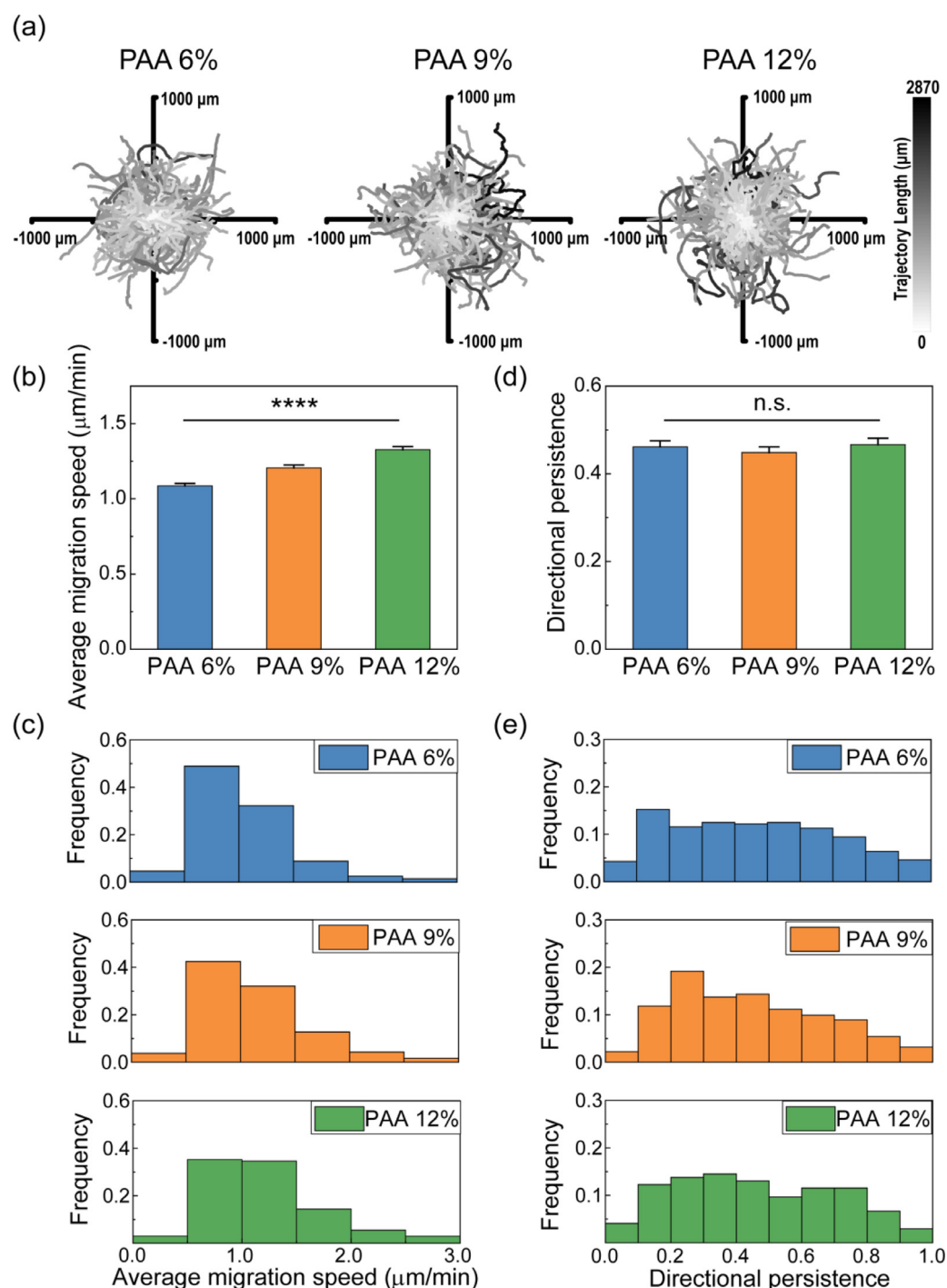


**Fig. 5.** Migration behavior of cells on hydrogels with different mesh sizes. (a) Migration trajectories of cells on different hydrogels ( $N > 269$  per group). (b) Average migration speed of cells on different hydrogels (Mean  $\pm$  SE,  $N > 269$  per group, one-way ANOVA,  $p < 0.0001$ ). (c) Distribution of average migration speed of cells on different hydrogels ( $N > 269$  per group). (d) Directional persistence of cells on different hydrogels (Mean  $\pm$  SE,  $N > 269$  per group, one-way ANOVA,  $p > 0.05$ ). (e) Distribution of directional persistence of cells on different hydrogels ( $N > 269$  per group).

phology of actin stress fibers, we stain the cells with fluorescent phalloidin. For cells on hydrogels with smaller meshes, more actin stress fibers are formed, as shown by the red fluorescent stain in Fig. 6(b). To investigate the focal adhesion of cells, we immunofluorescently label vinculin, one key structural protein of the focal adhesion [59–61], and quantify the morphology of focal adhesions with confocal microscopy. For all hydrogels, the focal adhesions display elongated shapes at the ends of the stress fibers, with a typical length of 3–5 μm, as shown by the green fluo-

rescent stain in Fig. 6(b). The morphology of these focal adhesions suggests that they are in the mature state, since unmaturing focal adhesions typically exhibit dot-like structures with lengths less than a micron [62,63]. The area of single focal adhesions increases as the hydrogel mesh size decreases, as shown in Fig. 6(c). Similarly, the number of focal adhesions per cell also increases, as shown in Fig. 6(d). As a consequence, the total focal adhesion area per cell increases dramatically as the hydrogel mesh size decreases, as shown in Fig. S8. Overall, our results suggest that the



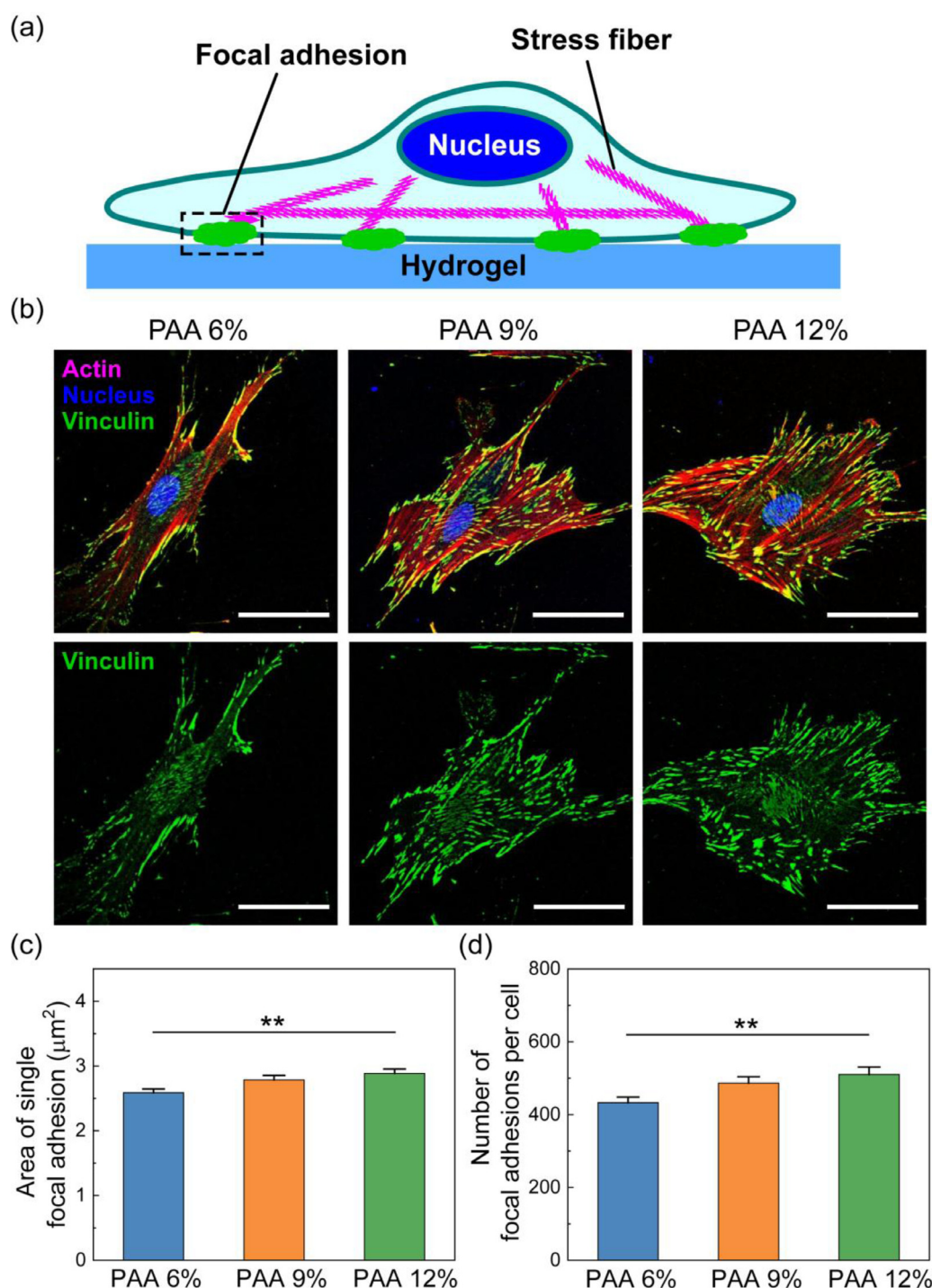


**Fig. 6.** Focal adhesions of cells on hydrogels with different mesh sizes. (a) Schematic of a spreading cell on the hydrogel substrate. The cell adheres to the hydrogel by forming focal adhesions, which are connected to actin stress fibers in the cell. (b) Representative confocal images of stress fibers and focal adhesions of cells on hydrogels with different mesh sizes. Actin is depicted in red; the nucleus is depicted in blue; and vinculin is depicted in green. Scale bars, 50  $\mu\text{m}$ . (c) Area of single focal adhesion of cells on hydrogels with different mesh sizes (Mean  $\pm$  SE,  $N > 88$  per group, one-way ANOVA,  $p < 0.01$ ). (d) Number of focal adhesions per cell on hydrogels with different mesh sizes (Mean  $\pm$  SE,  $N > 88$  per group, one-way ANOVA,  $p < 0.01$ ).

ability of cells to form focal adhesion is greatly promoted, and therefore a cell has better adhesion on hydrogels with smaller meshes, as evidenced by the increase of both the number and area of focal adhesion per cell. This also suggests that cells on hydrogels with smaller mesh sizes pull a larger amount of protein, given that the density of the collagen coating is similar among all substrates.

Interestingly, we find a close correlation between focal adhesion area and cell spreading area: cells with larger focal adhesions also tend to have larger spreading areas. This finding agrees with those found for cells on substrates with different stiffnesses [64], despite the fact that the variation here is the hydrogel mesh size rather than the stiffness. However, we observe a positive correlation between focal adhesion size and cell migration speed, which con-

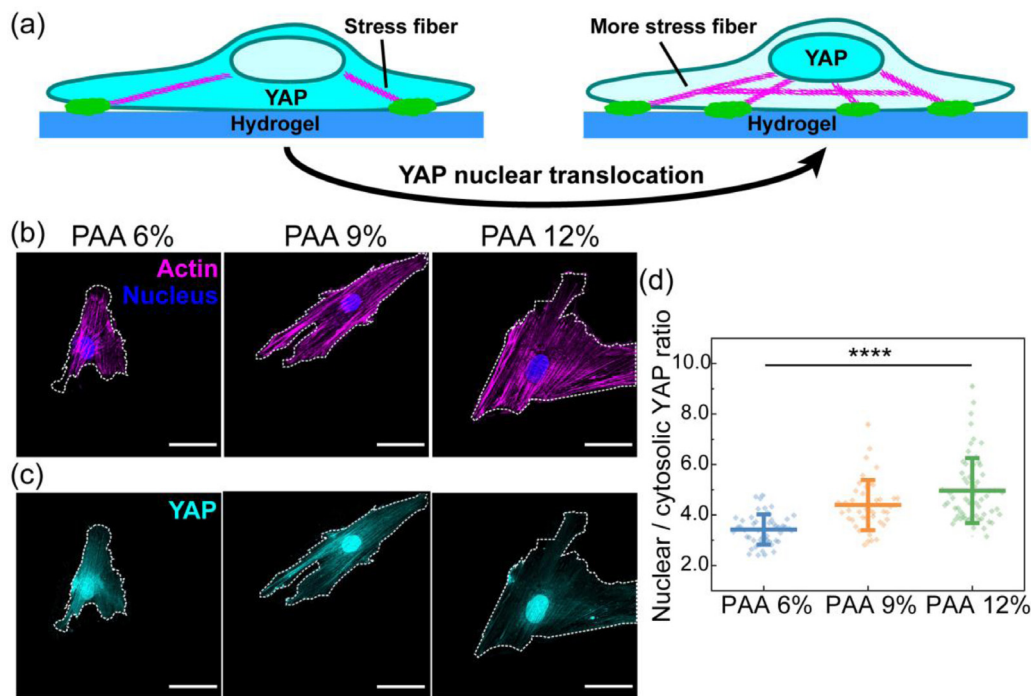


**Fig. 7.** YAP nuclear translocation of cells on hydrogels with different mesh sizes. (a) Schematic view of YAP nuclear translocation. As more stress fibers form in cells, YAP translocates from the cytoplasm to the nucleus of the cell. (b) Representative confocal fluorescence microscopy images of actin stress fibers in cells on hydrogels with different mesh sizes. The outline of the cell is represented by the white dashed line. Actin stress fibers are depicted in red; the nucleus is depicted in blue. Scale bars, 50  $\mu\text{m}$ . (c) Representative confocal fluorescence microscopy images of YAP in cells on hydrogels with different mesh sizes. The outline of the cell is represented by the white dashed line. YAP is depicted in cyan. Scale bars, 50  $\mu\text{m}$ . (d) The ratio of nuclear to cytosolic YAP for cells on hydrogels with different mesh sizes (Mean  $\pm$  SD,  $N > 42$  per group, one-way ANOVA,  $p < 0.0001$ ).

tradicts the biphasic correlation reported previously [65–68]. This likely indicates the focal adhesion size in our study is below the size threshold that inhibits cell migration and therefore positively correlates with cell migration speed.

### 3.7. Effect of hydrogel mesh size on the yes-associated protein (YAP) nuclear translocation

The key mechanism that regulates cell response to structural and mechanical cues is mechanotransduction [55,69]. To test whether that is the case for the measurements presented here, we quantify the distribution of yes-associated protein (YAP), a key transcriptional regulator that affects the mechanotransduction of cells by translocating from the cytoplasm to the nucleus [70–74]. The translocation of YAP is regulated by the tension of the F-actin cytoskeleton, which is usually correlated with the formation of stress fibers [75,76], as illustrated in Fig. 7(a). Therefore, we investigate actin and YAP in the cells with immunofluorescent staining and image them with confocal microscopy. As the mesh size of the hydrogel decreases, more stress fibers are formed in cells, as shown in Fig. 7(b). In addition, YAP becomes more localized in the nuclear region than the cytosolic region of the cell, as shown in Fig. 7(c). We quantify the total fluorescence intensity of YAP in the nucleus and cytosol of cells with ImageJ. The ratio of nuclear to cytosolic YAP increases for the cells grown on hydrogels with smaller meshes, as shown in Fig. 7(d). Our results suggest that the mesh size of the hydrogel alters YAP nuclear translocation and acts as a physical regulator that modulates cellular mechanotransduction.

When grown on stiffer substrates, cells have more YAP localized in the nucleus than in the cytoplasm [71,74]. They also show the enhanced formation of focal adhesions and stress fibers [73,77]. A possible explanation is that the increased tension exerted through focal adhesions by actomyosin stress fibers opens

the nuclear pores and thus allows the entry of YAP from the cytoplasm to the nucleus [76]. Interestingly, similar phenomena are also observed in our systems, suggesting that a similar mechanism of mechanotransduction is triggered by hydrogel mesh size.

## 4. Conclusions

In this study, we report a hydrogel system with independently tunable mesh size and stiffness, and use it to isolate the effect of hydrogel mesh size on the behavior of hBMSCs, including cell attachment, spreading, and migration. We show that varying the hydrogel mesh size affects a multitude of cell behavior: the spreading area, nuclear projected area, and migration speed of cells all increase significantly as the mesh size of the hydrogel decreases, while the cell attachment is not affected. At the subcellular scale, both the area and the number of focal adhesions increase as the mesh size of the hydrogel decreases. Furthermore, we find a striking increase in YAP nuclear translocation in cells on hydrogels with smaller meshes, indicating that cellular mechanotransduction is markedly modulated by the mesh size of the hydrogel.

In summary, our study shows that cells respond to the mesh size of hydrogel which is often overlooked in the studies of the cell-substrate interaction, and highlights the important role of mesh size as a structural cue in regulating cell behavior.

This study not only fills in a gap in knowledge in mechanobiology but also provides new insights to use the mesh size as a parameter to regulate cell behavior. Moreover, the results may help in optimizing the structural design of biomaterials in tissue engineering applications. Additionally, this work may deepen our understanding of the mechanics-dependent coordination of physiological and pathological tissue growth. In addition, our results may also be applicable for other fibroblasts, as they share similar phenotypic characteristics and similar responses in short-term assays

to mechanical cues [78–81]. Finally, the fundamental mechanisms by which the mesh size affects the cell behavior remain unclear. Possible mechanisms include its influence on nutrient waste diffusion [82] and the variations in the viscous properties of the hydrogel with microstructure [83,84]. It would be valuable to further explore the complete biological pathway related to hydrogel mesh size in the future.

### Declaration of Competing Interest

The authors declare that they have no known competing financial interests or personal relationships that could have appeared to influence the work reported in this paper.

### Acknowledgments

J.X., Z.Y.H., Y.Y. and D.A.W. acknowledge the financial support from the National Science Foundation of United States (DMR-1708729), the National Science Foundation through the Harvard University MRSEC of United States (DMR-2011754, and DMR-1420570), and the National Institutes of Health of United States (EB023287). Z.Y.L., Y.S. and X. Q.F. acknowledge the financial support from the National Natural Science Foundation of China (Nos. 11620101001, 11921002, and 042014002).

### Supplementary materials

Supplementary material associated with this article can be found, in the online version, at doi:[10.1016/j.actbio.2022.01.025](https://doi.org/10.1016/j.actbio.2022.01.025).

### References

- [1] R.O. Hynes, A. Naba, Overview of the matrisome—an inventory of extracellular matrix constituents and functions, *Cold Spring Harb. Perspect. Biol.* 4 (1) (2012) a004903.
- [2] T. Yeung, P.C. Georges, L.A. Flanagan, B. Marg, M. Ortiz, M. Funaki, N. Zahir, W.Y. Ming, V. Weaver, P.A. Janney, Effects of substrate stiffness on cell morphology, cytoskeletal structure, and adhesion, *Cell Motil. Cytoskeleton* 60 (1) (2005) 24–34.
- [3] S.R. Caliali, J.A. Burdick, A practical guide to hydrogels for cell culture, *Nat. Methods* 13 (5) (2016) 405–414.
- [4] M.W. Tibbitt, K.S. Anseth, Hydrogels as extracellular matrix mimics for 3D cell culture, *Biotechnol. Bioeng.* 103 (4) (2009) 655–663.
- [5] Y. Li, E. Kumacheva, Hydrogel microenvironments for cancer spheroid growth and drug screening, *Sci. Adv.* 4 (4) (2018) eaas8998.
- [6] A.J. Engler, S. Sen, H.L. Sweeney, D.E. Discher, Matrix elasticity directs stem cell lineage specification, *Cell* 126 (4) (2006) 677–689.
- [7] J. Li, D. Han, Y.P. Zhao, Kinetic behaviour of the cells touching substrate: the interfacial stiffness guides cell spreading, *Sci. Rep.* 4 (2014) 3910.
- [8] J.S. Park, J.S. Chu, A.D. Tsou, R. Diop, Z. Tang, A. Wang, S. Li, The effect of matrix stiffness on the differentiation of mesenchymal stem cells in response to TGF- $\beta$ , *Biomaterials* 32 (16) (2011) 3921–3930.
- [9] L.E. Dickinson, D.R. Rand, J. Tsao, W. Eberle, S. Gerecht, Endothelial cell responses to micropillar substrates of varying dimensions and stiffness, *J. Biomed. Mater. Res. A* 100 (6) (2012) 1457–1466.
- [10] K. Metavarayuth, P. Sitasuwan, X. Zhao, Y. Lin, Q. Wang, Influence of surface topographical cues on the differentiation of mesenchymal stem cells *in vitro*, *ACS Biomater. Sci. Eng.* 2 (2) (2016) 142–151.
- [11] M. Akhmanova, E. Osidak, S. Domogatsky, S. Rodin, A. Domogatskaya, Physical, spatial, and molecular aspects of extracellular matrix of *in vivo* niches and artificial scaffolds relevant to stem cells research, *Stem Cells Int.* (2015).
- [12] B. Trappmann, J.E. Gautrot, J.T. Connelly, D.G. Strange, Y. Li, M.L. Oyen, M.A. Cohen Stuart, H. Boehm, B. Li, V. Vogel, J.P. Spatz, F.M. Watt, W.T. Huck, Extracellular-matrix tethering regulates stem-cell fate, *Nat. Mater.* 11 (7) (2012) 642–649.
- [13] J.H. Wen, L.G. Vincent, A. Fuhrmann, Y.S. Choi, K.C. Hribar, H. Taylor-Weiner, S. Chen, A.J. Engler, Interplay of matrix stiffness and protein tethering in stem cell differentiation, *Nat. Mater.* 13 (10) (2014) 979–987.
- [14] M. Rubinstein, R.H. Colby, *Polymer physics*, Oxford University Press New York, 2003.
- [15] B.V. Slaughter, S.S. Khurshid, O.Z. Fisher, A. Khademhosseini, N.A. Peppas, Hydrogels in regenerative medicine, *Adv. Mater.* 21 (32–33) (2009) 3307–3329.
- [16] M.C. LaPlaca, V.N. Vernekar, J.T. Shoemaker, D.K. Cullen, Three-dimensional neuronal cultures, in: *Methods in Bioengineering: 3D Tissue Engineering*, 2010, pp. 187–204.
- [17] E.R. Aurand, K.J. Lampe, K.B. Bjugstad, Defining and designing polymers and hydrogels for neural tissue engineering, *Neurosci. Res.* 72 (3) (2012) 199–213.
- [18] U. Horzum, B. Ozdil, D. Pesen-Okvur, Step-by-step quantitative analysis of focal adhesions, *MethodsX* 1 (2014) 56–59.
- [19] J.H. McDonald, *Handbook of Biological Statistics*, Sparky House Publishing Baltimore, MD2009.
- [20] N.C. Stellwagen, E. Stellwagen, Effect of the matrix on DNA electrophoretic mobility, *J. Chromatogr. A* 1216 (10) (2009) 1917–1929.
- [21] N.C. Stellwagen, Effect of the electric-field on the apparent mobility of large DNA fragments in agarose gels, *Biopolymers* 24 (12) (1985) 2243–2255.
- [22] A.G. Ogston, The spaces in a uniform random suspension of fibres, *Trans. Faraday Soc.* 54 (11) (1958) 1754–1757.
- [23] M. Galli, M. Oyen, Spherical indentation of a finite poroelastic coating, *Appl. Phys. Lett.* 93 (3) (2008) 031911.
- [24] A. Buxboim, K. Rajagopal, A.E. Brown, D.E. Discher, How deeply cells feel: methods for thin gels, *J. Phys. Condens. Matter* 22 (19) (2010) 194116.
- [25] E.K. Dimitriadis, F. Horkay, J. Maresca, B. Kachar, R.S. Chadwick, Determination of elastic moduli of thin layers of soft material using the atomic force microscope, *Biophys. J.* 82 (5) (2002) 2798–2810.
- [26] A.A. Khalili, M.R. Ahmad, A review of cell adhesion studies for biomedical and biological applications, *Int. J. Mol. Sci.* 16 (8) (2015) 18149–18184.
- [27] J.P. Stegemann, H. Hong, R.M. Nerem, Mechanical, biochemical, and extracellular matrix effects on vascular smooth muscle cell phenotype, *J. Appl. Physiol.* 98 (6) (1985) 2321–2327 2005.
- [28] Y. Artemenko, L. Axiotakis, J. Borleis, P.A. Iglesias, P.N. Devreotes, Chemical and mechanical stimuli act on common signal transduction and cytoskeletal networks, *Proc. Natl. Acad. Sci. U. S. A.* 113 (47) (2016) E7500–E7509.
- [29] C. Gaudet, W.A. Marganski, S. Kim, C.T. Brown, V. Gunderia, M. Dembo, J.Y. Wong, Influence of type I collagen surface density on fibroblast spreading, motility, and contractility, *Biophys. J.* 85 (5) (2003) 3329–3335.
- [30] A. Engler, L. Bacakova, C. Newman, A. Hategan, M. Griffin, D. Discher, Substrate compliance versus ligand density in cell on gel responses, *Biophys. J.* 86 (1) (2004) 617–628.
- [31] A.J. Engler, L. Richert, J.Y. Wong, C. Picart, D.E. Discher, Surface probe measurements of the elasticity of sectioned tissue, thin gels and polyelectrolyte multilayer films: Correlations between substrate stiffness and cell adhesion, *Surf. Sci.* 570 (1–2) (2004) 142–154.
- [32] J.P. Orgel, A. Miller, T.C. Irving, R.F. Fischetti, A.P. Hammersley, T.J. Wess, The *in situ* supermolecular structure of type I collagen, *Structure* 9 (11) (2001) 1061–1069.
- [33] M. Gale, M.S. Pollanen, P. Markiewicz, M.C. Goh, Sequential assembly of collagen revealed by atomic force microscopy, *Biophys. J.* 68 (5) (1995) 2124–2128.
- [34] J.K. Mouw, G. Ou, V.M. Weaver, Extracellular matrix assembly: a multiscale deconstruction, *Nat. Rev. Mol. Cell Biol.* 15 (12) (2014) 771–785.
- [35] J.P. Lee, E. Kassianidou, J.L. MacDonald, M.B. Francis, S. Kumar, N-terminal specific conjugation of extracellular matrix proteins to 2-pyridinedicarboxaldehyde functionalized polyacrylamide hydrogels, *Biomaterials* 102 (2016) 268–276.
- [36] T. Gurry, P.S. Nerenberg, C.M. Stultz, The contribution of interchain salt bridges to triple-helical stability in collagen, *Biophys. J.* 98 (11) (2010) 2634–2643.
- [37] W.J. Hadden, J.L. Young, A.W. Holle, M.L. McFetridge, D.Y. Kim, P. Wijesinghe, H. Taylor-Weiner, J.H. Wen, A.R. Lee, K. Bieback, Stem cell migration and mechanotransduction on linear stiffness gradient hydrogels, *Proc. Natl. Acad. Sci. U. S. A.* 114 (22) (2017) 5647–5652.
- [38] B.C. Isenberg, P.A. Dimilla, M. Walker, S. Kim, J.Y. Wong, Vascular smooth muscle cell durotaxis depends on substrate stiffness gradient strength, *Biophys. J.* 97 (5) (2009) 1313–1322.
- [39] A.E. Stanton, X. Tong, F. Yang, Varying solvent type modulates collagen coating and stem cell mechanotransduction on hydrogel substrates, *APL Bioeng.* 3 (3) (2019) 036108.
- [40] J.L. McGrath, Cell spreading: the power to simplify, *Curr. Biol.* 17 (10) (2007) R357–R358.
- [41] J. Folkman, A. Moscona, Role of cell shape in growth control, *Nature* 273 (5661) (1978) 345–349.
- [42] C.S. Chen, M. Mrksich, S. Huang, G.M. Whitesides, D.E. Ingber, Geometric control of cell life and death, *Science* 276 (5317) (1997) 1425–1428.
- [43] M. Guo, A.F. Pegoraro, A. Mao, E.H. Zhou, P.R. Arany, Y. Han, D.T. Burnette, M.H. Jensen, K.E. Kasza, J.R. Moore, F.C. Mackintosh, J.J. Fredberg, D.J. Mooney, J. Lippincott-Schwartz, D.A. Weitz, Cell volume change through water efflux impacts cell stiffness and stem cell fate, *Proc. Natl. Acad. Sci. U. S. A.* 114 (41) (2017) E8618–E8627.
- [44] R. Vishavkarma, S. Raghavan, C. Kuyyamadhi, A. Majumder, J. Dhawan, P.A. Pullarkat, Role of actin filaments in correlating nuclear shape and cell spreading, *PLoS One* 9 (9) (2014) e107895.
- [45] J. Xia, Y. Yuan, H. Wu, Y. Huang, D.A. Weitz, Decoupling the effects of nanopore size and surface roughness on the attachment, spreading and differentiation of bone marrow-derived stem cells, *Biomaterials* 248 (2020) 120014.
- [46] K. Webb, V. Hlady, P.A. Tresco, Relationships among cell attachment, spreading, cytoskeletal organization, and migration rate for anchorage-dependent cells on model surfaces, *J. Biomed. Mater. Res.* 49 (3) (2000) 362–368.
- [47] D.A. Lauffenburger, A.F. Horwitz, Cell migration: a physically integrated molecular process, *Cell* 84 (3) (1996) 359–369.
- [48] A.J. Ridley, M.A. Schwartz, K. Burridge, R.A. Firtel, M.H. Ginsberg, G. Borisy, J.T. Parsons, A.R. Horwitz, Cell migration: integrating signals from front to back, *Science* 302 (5651) (2003) 1704–1709.
- [49] D.R. Nisbet, J.S. Forsythe, W. Shen, D.I. Finkelstein, M.K. Horne, Review paper: a review of the cellular response on electrospun nanofibers for tissue engineering, *J. Biomater. Appl.* 24 (1) (2009) 7–29.



- [50] K. Kolind, K.W. Leong, F. Besenbacher, M. Foss, Guidance of stem cell fate on 2D patterned surfaces, *Biomaterials* 33 (28) (2012) 6626–6633.
- [51] J. Wang, J.W. Petefish, A.C. Hillier, I.C. Schneider, Epitaxially grown collagen fibrils reveal diversity in contact guidance behavior among cancer cells, *Langmuir* 31 (1) (2015) 307–314.
- [52] B.D. Harms, G.M. Bassi, A.R. Horwitz, D.A. Lauffenburger, Directional persistence of EGF-induced cell migration is associated with stabilization of lamellipodial protrusions, *Biophys. J.* 88 (2) (2005) 1479–1488.
- [53] M. Krause, A. Gautreau, Steering cell migration: lamellipodium dynamics and the regulation of directional persistence, *Nat. Rev. Mol. Cell Biol.* 15 (9) (2014) 577–590.
- [54] D.E. Discher, P. Janmey, Y.L. Wang, Tissue cells feel and respond to the stiffness of their substrate, *Science* 310 (5751) (2005) 1139–1143.
- [55] D.E. Jaalouk, J. Lammerding, Mechanotransduction gone awry, *Nat. Rev. Mol. Cell Biol.* 10 (1) (2009) 63–73.
- [56] S. Tojkander, G. Gateva, P. Lappalainen, Actin stress fibers—assembly, dynamics and biological roles, *J. Cell Sci.* 125 (Pt 8) (2012) 1855–1864.
- [57] N.D. Gallant, K.E. Michael, A.J. Garcia, Cell adhesion strengthening: contributions of adhesive area, integrin binding, and focal adhesion assembly, *Mol. Biol. Cell* 16 (9) (2005) 4329–4340.
- [58] K.E. Michael, A.J. Garcia, Cell adhesion strengthening: measurement and analysis, *Cell Mech.* (2007) 329–346.
- [59] K. Haase, Z. Al-Rekabi, A.E. Pelling, Mechanical cues direct focal adhesion dynamics, *Prog. Mol. Biol. Transl. Sci.* 126 (2014) 103–134.
- [60] K. Hayakawa, H. Tatsumi, M. Sokabe, Mechano-sensing by actin filaments and focal adhesion proteins, *Commun. Integr. Biol.* 5 (6) (2012) 572–577.
- [61] G.R. Owen, D. Meredith, R. Richards, Focal adhesion quantification—a new assay of material biocompatibility? Review, *Eur. Cells Mater.* 9 (2005) 85–96 discussion 85–96.
- [62] M.A. Partridge, E.E. Marcantonio, Initiation of attachment and generation of mature focal adhesions by integrin-containing filopodia in cell spreading, *Mol. Biol. Cell* 17 (10) (2006) 4237–4248.
- [63] C.W. Kuo, D.Y. Chueh, P. Chen, Investigation of size-dependent cell adhesion on nanostructured interfaces, *J. Nanobiotechnol.* 12 (2014) 54.
- [64] D.H. Kim, D. Wirtz, Predicting how cells spread and migrate: focal adhesion size does matter, *Cell Adhes. Migr.* 7 (3) (2013) 293–296.
- [65] D.H. Kim, D. Wirtz, Focal adhesion size uniquely predicts cell migration, *FASEB J.* 27 (4) (2013) 1351–1361.
- [66] S.P. Palecek, J.C. Loftus, M.H. Ginsberg, D.A. Lauffenburger, A.F. Horwitz, Integrin-ligand binding properties govern cell migration speed through cell-substratum adhesiveness, *Nature* 385 (6616) (1997) 537–540.
- [67] G. Maheshwari, G. Brown, D.A. Lauffenburger, A. Wells, L.G. Griffith, Cell adhesion and motility depend on nanoscale RGD clustering, *J. Cell Sci.* 113 (10) (2000) 1677–1686.
- [68] P.A. DiMilla, K. Barbee, D.A. Lauffenburger, Mathematical model for the effects of adhesion and mechanics on cell migration speed, *Biophys. J.* 60 (1) (1991) 15–37.
- [69] Y. Sun, C.S. Chen, J. Fu, Forcing stem cells to behave: a biophysical perspective of the cellular microenvironment, *Annu. Rev. Biophys.* 41 (2012) 519–542.
- [70] A. Totaro, T. Panciera, S. Piccolo, YAP/TAZ upstream signals and downstream responses, *Nat. Cell Biol.* 20 (8) (2018) 888–899.
- [71] S. Dupont, Role of YAP/TAZ in cell-matrix adhesion-mediated signalling and mechanotransduction, *Exp. Cell. Res.* 343 (1) (2016) 42–53.
- [72] S.E. Hiemer, A.D. Szymaniak, X. Varelas, The transcriptional regulators TAZ and YAP direct transforming growth factor beta-induced tumorigenic phenotypes in breast cancer cells, *J. Biol. Chem.* 289 (19) (2014) 13461–13474.
- [73] G. Nardone, J. Oliver-De La Cruz, J. Vrbsky, C. Martini, J. Pribyl, P. Skladal, M. Pesl, G. Caluori, S. Pagliari, F. Martino, Z. Maceckova, M. Hajdud, A. Sanz-Garcia, N.M. Pugno, G.B. Stokin, G. Forte, YAP regulates cell mechanics by controlling focal adhesion assembly, *Nat. Commun.* 8 (2017) 15321.
- [74] S. Dupont, L. Morsut, M. Aragona, E. Enzo, S. Giullitti, M. Cordenonsi, F. Zanconato, J.Le Digabel, M. Forcato, S. Bicciato, N. Elvassore, S. Piccolo, Role of YAP/TAZ in mechanotransduction, *Nature* 474 (7350) (2011) 179–183.
- [75] K. Wada, K. Itoga, T. Okano, S. Yonemura, H. Sasaki, Hippo pathway regulation by cell morphology and stress fibers, *Development* 138 (18) (2011) 3907–3914.
- [76] A. Elosegui-Artola, I. Andreu, A.E.M. Beedle, A. Lezamiz, M. Uroz, A.J. Kosmalska, R. Oria, J.Z. Kechagia, P. Rico-Lastres, A.L. Le Roux, C.M. Shanahan, X. Trepas, D. Navajas, S. Garcia-Manyès, P. Roca-Cusachs, Force triggers YAP nuclear entry by regulating transport across nuclear pores, *Cell* 171 (6) (2017) 1397–1410 e14.
- [77] S. Fusco, V. Panzetta, P.A. Netti, Mechanosensing of substrate stiffness regulates focal adhesions dynamics in cell, *Meccanica* 52 (14) (2017) 3389–3398.
- [78] B. Venugopal, P. Mogha, J. Dhawan, A. Majumder, Cell density overrides the effect of substrate stiffness on human mesenchymal stem cells' morphology and proliferation, *Biomater. Sci.* 6 (5) (2018) 1109–1119.
- [79] A. Chopra, M.E. Murray, F.J. Byfield, M.G. Mendez, R. Halleluyan, D.J. Restle, D.R.B. Aroush, P.A. Galie, K. Pogoda, R. Bucki, Augmentation of integrin-mediated mechanotransduction by hyaluronic acid, *Biomaterials* 35 (1) (2014) 71–82.
- [80] M. Guo, A.F. Pegoraro, A. Mao, E.H. Zhou, P.R. Arany, Y. Han, D.T. Burnette, M.H. Jensen, K.E. Kasza, J.R. Moore, Cell volume change through water efflux impacts cell stiffness and stem cell fate, *Proc. Natl. Acad. Sci.* 114 (41) (2017) E8618–E8627.
- [81] R.A. Denu, S. Nemcek, D.D. Bloom, A.D. Goodrich, J. Kim, D.F. Mosher, P. Hematti, Fibroblasts and mesenchymal stromal/stem cells are phenotypically indistinguishable, *Acta Haematol.* 136 (2) (2016) 85–97.
- [82] H. Yu, I. Meyvantsson, I.A. Shkel, D.J. Beebe, Diffusion dependent cell behavior in microenvironments, *Lab Chip* 5 (10) (2005) 1089–1095.
- [83] J.M. Grolman, P. Weinand, D.J. Mooney, Extracellular matrix plasticity as a driver of cell spreading, *Proc. Natl. Acad. Sci.* 117 (42) (2020) 25999–26007.
- [84] O. Chaudhuri, L. Gu, D. Klumpers, M. Darnell, S.A. Bencherif, J.C. Weaver, N. Huebsch, H.P. Lee, E. Lippens, G.N. Duda, D.J. Mooney, Hydrogels with tunable stress relaxation regulate stem cell fate and activity, *Nat. Mater.* 15 (3) (2016) 326–334.